



Customized physical and structural features of phosphate-based glass-ceramics: role of Ag nanoparticles and Ho³⁺ impurities

Areej S. Alqarni , R. Hussin , S. N. Alamri & S. K. Ghoshal

To cite this article: Areej S. Alqarni , R. Hussin , S. N. Alamri & S. K. Ghoshal (2020) Customized physical and structural features of phosphate-based glass-ceramics: role of Ag nanoparticles and Ho³⁺ impurities, Journal of Taibah University for Science, 14:1, 954-962, DOI: [10.1080/16583655.2020.1791536](https://doi.org/10.1080/16583655.2020.1791536)

To link to this article: <https://doi.org/10.1080/16583655.2020.1791536>



© 2020 The Author(s). Published by Informa UK Limited, trading as Taylor & Francis Group



Published online: 12 Jul 2020.



Submit your article to this journal [↗](#)



Article views: 92





View related articles [↗](#)



View Crossmark data [↗](#)

Customized physical and structural features of phosphate-based glass-ceramics: role of Ag nanoparticles and Ho³⁺ impurities

Areej S. Alqarni ^{a,b}, R. Hussin^a, S. N. Alamri^b and S. K. Ghoshal ^a

^aDepartment of Physics, Faculty of Science, Universiti Teknologi Malaysia, Johor, Malaysia; ^bDepartment of Physics, Faculty of Science, Taibah University, Madinah, Saudi Arabia

ABSTRACT

The effects of silver nanoparticles (Ag NPs) embedment on the physical and structural characteristics of the holmium ions (Ho³⁺) activated phosphate-based glass-ceramics were assessed. Two series of such glass-ceramics were prepared using the melt-quenching and characterized. In the first series, the Ag NPs were nucleated from the incorporated AgCl via the redox process. In the second series, the pure Ag nanopowder was directly added. The overall properties of these glass-ceramics were strongly sensitive to the cooling procedure and NPs addition strategies, leading to different density and refractive index modifications in the two series. The recorded O 1s XPS peaks were exploited to determine the bridging to non-bridging oxygen ratios in the studied glass-ceramics network that enabled to unfold the differences in the observed inferences. A compelling correlation among various attributes in the achieved glass-ceramics was established. Briefly, the overall traits of the proposed glass-ceramics were tailored by regulating the preparation conditions.

ARTICLE HISTORY

Received 17 February 2020
Revised 1 May 2020
Accepted 11 May 2020

KEYWORDS


Holmium ion; glass-ceramic; silver nanoparticles; refractive index; metallization criterion; polarizability

1. Introduction

The oxide glasses and glass-ceramics doped with lanthanides ions (LIs) are prospective for many applications such as optical fibres, waveguides, lasers amplifiers, sensors, light emitting diodes, and displays [1–3]. The boro-phosphate system as the host is preferred for the impurities doping due to its distinct structural properties compared to the pure borate or phosphate systems [4–6]. It was reported that the incorporation of the sulphate ions can offer an ideal environment for the large intake of LIs that is advantageous for the reduction of the LIs clustering and design of the miniaturized lasers [7]. Some studies also demonstrated that the chemical durability and structural stability of the boro-phosphate network can be improved via the incorporation of the zinc ions [8,9]. Holmium ions (Ho³⁺) are the potential candidates for the wide range of applications such as the optical data storage, sensors, lasers, amplifiers, and radars [10–12]. It has unique 4f energy levels (several excited states with high energies) that are desired for the exclusive luminescence transitions. Nevertheless, the non-radiative relaxation processes associated to various excited states contributes to the energy loss, thereby limiting its practical applications [9]. To surmount such shortcomings an appropriate selection of the host matrix is necessary where the local electric field inside the host network is responsible for the splitting of the 4f energy levels of Ho³⁺ [13,14]. Thus, the selection of the host, sensitization by

plasmonic nanostructures and composition optimization are the effective strategies to modify the overall properties, thus achieving the best luminescence features of the Ho³⁺.

Silver nanoparticles (Ag NPs) are the common plasmonic metamaterial which are abundant, biocompatible, chemically stable and resistant to oxidation. Thus, Ag NPs have been used as the sensitizers in many systems to improve the LI's optical properties [15–19]. In the host matrix these Ag NPs can be embedded by two ways, where their nucleation and growth in both cases follow the Ostwald ripening and coalescence mechanisms [20,21]. In the first mode, an appropriate amount of chloride, nitride, carbonate or oxide of silver is mixed into the glass composition as constituent and then the Ag NPs are formed by the redox reactions during the annealing at high temperature [22–25]. In the other approach, pure silver nanopowder is added directly into the constituent mixture where the NPs from the powder are dispersed into the host matrix during thermal treatment without further redox process. It is worth mentioning that the application prospect of the Ag NPs and Ho³⁺ incorporated zinc-sulfo-boro-phosphate glass-ceramic system has not been completely explored yet. This requires fundamental understanding of the role played by the included Ag NPs and Ho³⁺ in improving various physical, structural, and optical properties of the resultant zinc-sulfo-boro-phosphate glass-ceramic material.

CONTACT S. K. Ghoshal  sibkrishna@utm.my

The density of the glasses and glass-ceramics is the most simple and highly informative physical property that can be measured. In addition, the network structure can be explained in terms of molar volume rather than density, as the former deals the spatial distribution of the ions forming the structure under study. The polaron (quasi-particle) concept has been studied in both ordered and disordered solids to understand the interactions between electrons and atoms or ions in the solid materials. The polaron radius (r_p) must be greater than the radius of the atom in which the electron is localized, but smaller than the inter-nuclear distance (r_i), separating these sites. Moreover, the covalency and electrovalency of the network can be predicted through the field strength of the LIs. The molar refractivity is a critical property determined from an optical (refractive index) and structural (density and average molecular weight) quantities and describes the polarizability of the material [26–28].

In the present work, the structural properties based in the above-mentioned physical parameters of the Ho^{3+} activated zinc-sulfo-boro-phosphate glass-ceramic containing different amounts of Ag NPs were studied. The variation of those physical parameters as a function of Ag NPs content (two cases) was determined. The first case illustrated the impact of Ag NPs which formed from AgCl while the second case depicted the effect of Ag NPs obtained from pure Ag nanopowder. Density and refractive index of all samples were measured and used to calculate the cited physical parameters. The estimated data were plotted, discussed, and correlated.

2. Experimental and theoretical

Two series of phosphate-based glass-ceramics incorporated with different amount of Ag NPs content (from two different chemical sources) were prepared using the melt-quenching method. An analytical grade H_3PO_4 , B_2O_3 , $\text{ZnSO}_4 \cdot 7\text{H}_2\text{O}$, Ho_2O_3 , AgCl, and pure Ag nanopowder were used as raw materials. First, an appropriate amount of the raw constituent materials (as per the molar formula given in Table 1) were accurately weighting by a digital balance. Then the constituents

(batch) were very well mixed to assure the homogeneity. Next, the mixture (inside an alumina crucible) transferred to an electrical furnace operated at 300 °C for 30 min. After that, the dried mixture was placed inside another furnace (operated at 1300 °C for 90 min) for complete the melting process. Then, the melt was poured on a stainless-steel plate inside a furnace at 300 °C and annealed for 2 h to assist the formation of some crystalline phase within the amorphous structure. Finally, the solidified sample was left (inside the turn-off annealing furnace) to cool down naturally to room temperature.

Figure 1 describes the thermal treatment schedule of the prepared samples. The physical appearance of as-quenched glass-ceramics is shown in the inset of Figure 1. Density of all the samples (Table 1) was measured using Archimedes method (using toluene as an immersion liquid). The refractive index was measured using Atago-Abbe refractometer (589 nm) at room temperature. The microstructures of the prepared samples were imaged and the selected area electron diffraction (SAED) patterns were taken using a high resolution transmission electron microscope (HRTEM and EDX, Jeol-ARM200F operated at 200 kV). The SAED patterns were analysed by Gatan digital micrograph software. X-ray photoelectron spectrometer (XPS, Shimadzu AXIS Ultra^{DLD}) was used to detect the elemental compositions of the prepared samples at the surface level. XPS spectral data analyses were performed by CasaXPS software. The physical properties were calculated based on the linearized density and refractive index values using the mathematical formulas listed in Table 2. The samples prepared using AgCl and pure Ag nanopowder as starting material are called Series I and Series II, respectively.

3. Results and discussion

Figures 2(a) and 3(a) depict the TEM images of the ZBPHA0.8 (Series I) and ZBHPA0.8 (Series II) sample, respectively. Herein, two significant observations can be made: (i) the glass-ceramic nature of the proposed systems (small dark spots on the amorphous backdrop

Table 1. Samples code, compositions, densities, and measured refractive indices.

Sample code	Composition (mol%)						Density (g cm^{-3})	Refractive index
	ZnSO ₄	B ₂ O ₃	P ₂ O ₅	Ho ₂ O ₃	AgCl	Pure Ag		
Series I								
ZBPHA0.6	30	30	38.9	0.5	0.6	–	2.906	1.6544
ZBPHA0.7	30	30	39.8	0.5	0.7	–	2.848	1.6547
ZBPHA0.8	30	30	39.7	0.5	0.8	–	2.854	1.6546
ZBPHA0.9	30	30	39.6	0.5	0.9	–	2.896	1.6545
Series II								
ZBHPA0.6	30	30	38.9	0.5	–	0.6	2.791	1.6543
ZBHPA0.7	30	30	39.8	0.5	–	0.7	2.800	1.6542
ZBHPA0.8	30	30	39.7	0.5	–	0.8	2.853	1.6541
ZBHPA0.9	30	30	39.6	0.5	–	0.9	2.833	1.6542

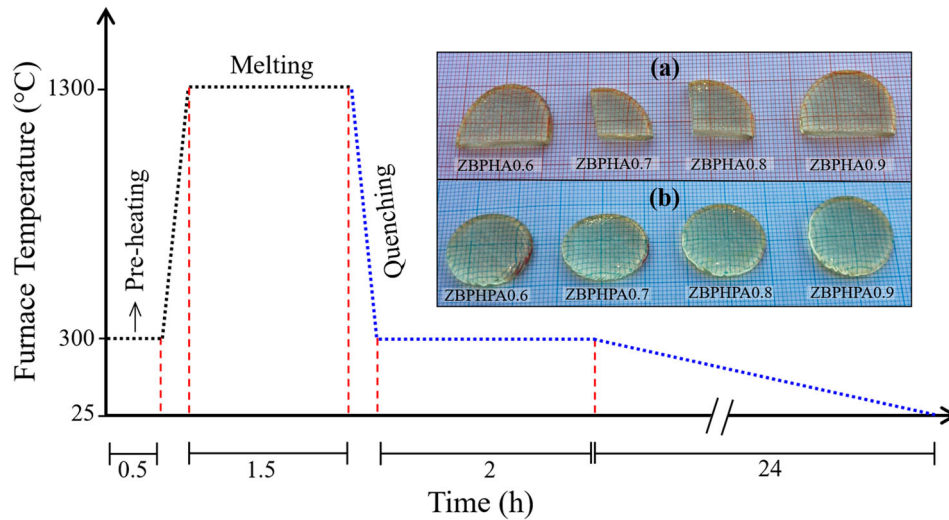


Figure 1. The glass-ceramics preparation thermal history. Inset: the physical appearance of the prepared samples under natural light (a) Series I, and (b) Series II.

Table 2. The formulas used for the physical properties calculation [27–30].

Term	Symbol (unit)	Formula	Related terms
Density	ρ (g cm ⁻³)	$\rho = \frac{W_a}{W_a - W_t} \rho_t$	W_a : Weights of the sample in air. W_t : Weights of the sample in toluene. ρ_t : Density of toluene.
Average molecular weight	M_{av} (g)	$M_{av} = \frac{1}{100} \sum_i x_i m_i$	x_i : Mole fraction of each component i in the composition. m : Molar mass of each component i in the composition.
Molar volume	V_m (cm ³ mol ⁻¹)	$V_m = \frac{M_{av}}{\rho}$	
Lls concentration	N	$N = \frac{\text{mol\% of Lls} \times \rho \times N_A}{M_{av}}$	N_A : Avogadro's number.
Inter-nuclear distance	r_i (Å)	$r_i = \left(\frac{1}{N}\right)^{1/3}$	
Polaron radius	r_p (Å)	$r_p = \frac{1}{2} \left(\frac{\pi}{6N}\right)^{1/3}$	
Field strength	F (cm ⁻²)	$F = \frac{Z}{r_p^2}$	Z : Atomic number of Lls. r_p : Polaron radius.
Molar refractivity	R_m (cm ³)	$R_m = \frac{n^2 - 1}{n^2 + 2} V_m$	n : Refractive index.
Molar polarizability	α_m (Å ³)	$\alpha_m = \frac{3R_m}{4\pi N_A}$	
Metallization criterion	M	$M = 1 - \frac{R_m}{V_m}$	

[31]), and (ii) the existence of the Ag NPs in the network structure (large dark spots). These disclosures were confirmed by the SAED patterns of the dark spots, where the SAED pattern of the small dark spots (upper insets of Figures 2(a) and 3(a)) demonstrated a strong evidence of the emergence of the B₂O₃ nanocrystalline phase within the disordered matrix. A reflection from (310) lattice plane of the B₂O₃ was matched to the ICDD number 00-006-0297 and consistent with the XRD pattern of the undoped (39.5P₂O₅ – 30B₂O₃ – 30ZnSO₄ – 0.5Ho₂O₃) sample as reported earlier [31]. Similarly, the SAED pattern of the big dark spots (lower insets of Figures 2(a) and 3(a)) authenticated the presence of Ag NPs in the host matrix. The obtained reflections from the Ag (002) and (110) lattice plane in the ZBPHA0.8

sample were matched to the ICDD number 01-071-5025 while a reflection from the Ag (200) lattice plane in the ZBPHA0.8 sample was matched to the ICDD number 03-065-8428.

The histogram in Figure 2(b) and (c) shows the corresponding average crystallite size of the B₂O₃ (b) and Ag NPs (c) for the ZBPHA0.8 (Series I) sample. Likewise, Figure 3(b) and (c) shows the corresponding average crystallite size of the B₂O₃ (b) and Ag NPs (c) for the ZBPHA0.8 (Series II) sample. The estimated average nanocrystallite size of the B₂O₃ for the ZBPHA0.8 and ZBPHA0.8 sample was approximately 4.2 and 4.5 nm, respectively. The mean Ag NPs size was approximately 18.4 nm (for ZBPHA0.8 sample) and 7.9 nm (for ZBPHA0.8 sample).

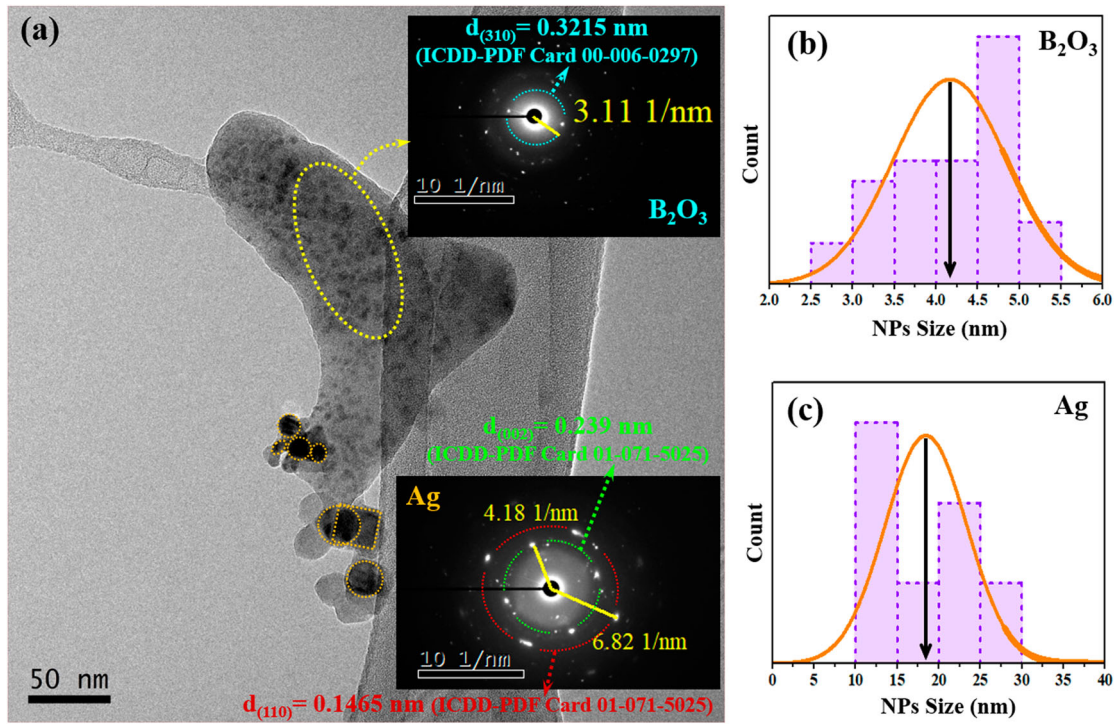


Figure 2. (a) TEM image of ZBPHA0.8 (Series I) sample. The upper and lower insets are the respective SAED patterns of the small and big dark spots. (b) and (c) represent the corresponding crystallite size distribution of the small and big dark spots.

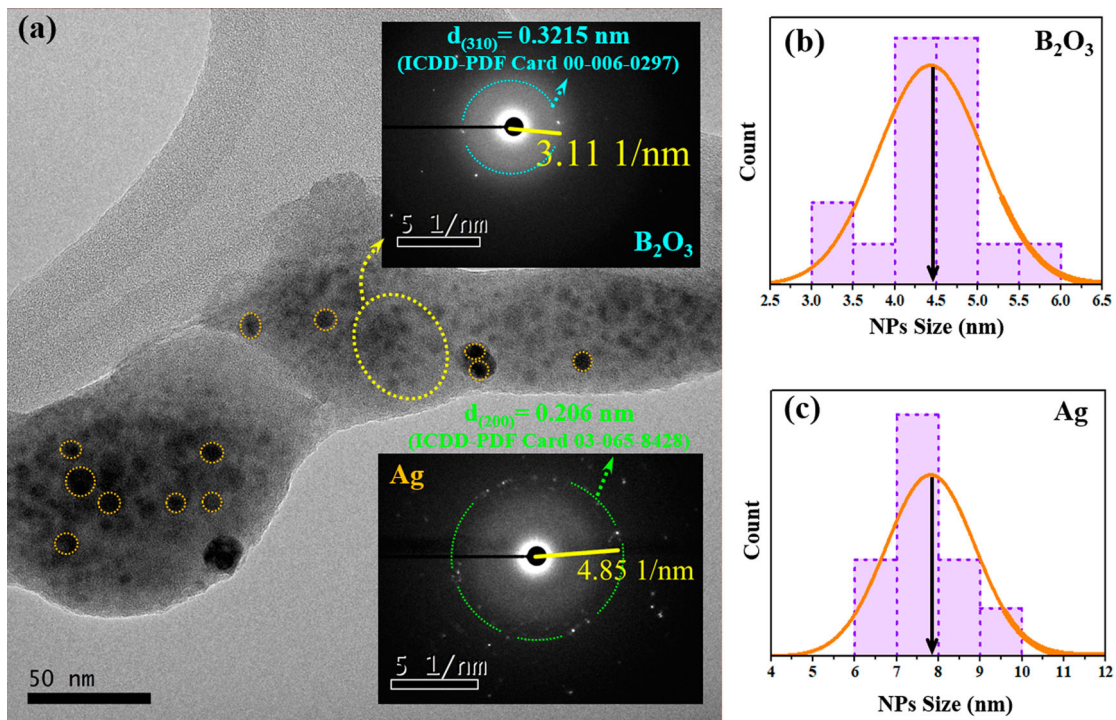


Figure 3. (a) TEM image of ZBPHA0.8 (Series II) sample. The upper and lower insets are the respective SAED patterns of the small and big dark spots. (b) and (c) indicate the corresponding crystallite size distribution of the small and big dark spots.

To reconfirm the achievement of the optimum phase for the proposed system, the undoped sample was synthesized with an extremely rapid quenching (inset of Figure 4). The XRD measurements (Shimadzu 6100 diffractometer) for different portions from the latter sample exposed a totally glass pattern as depicted in Figure 4. However, the titled series of Ag NPs doped phosphate-based glass-ceramic were

obtained by the slower cooling procedure (Figure 1). In this procedure, the formation of the crystalline domains within the amorphous matrix was proven to be highly probable [32]. Moreover, referring to the physical appearance of the obtained samples (inset of Figure 1) the slower cooling procedure was assisted the release of the thermal strains before cooling down to room temperature, resulting in a non-cracked

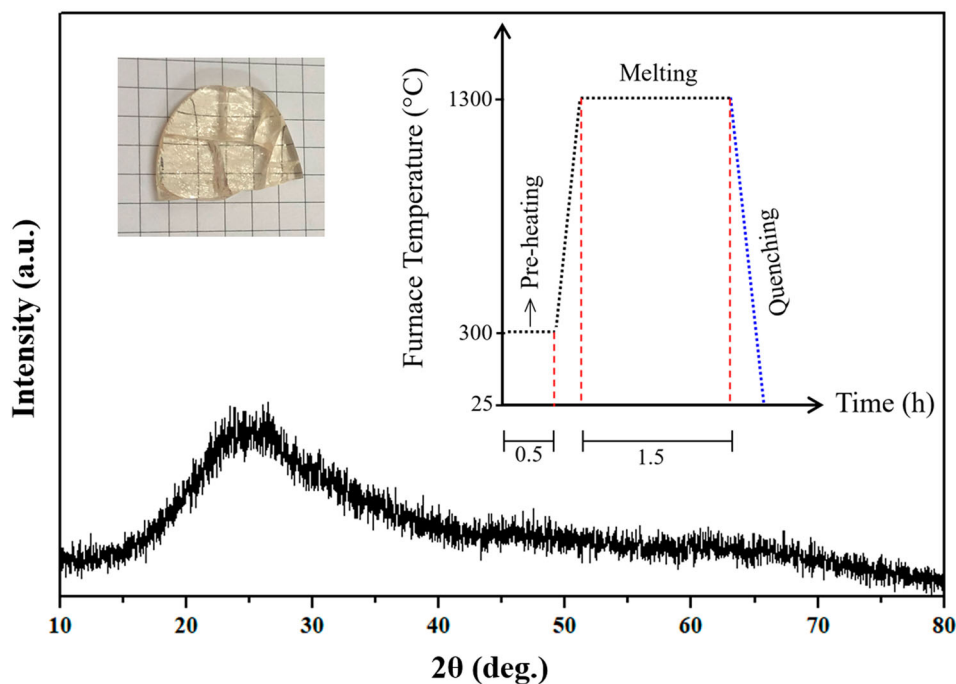


Figure 4. The XRD pattern of the undoped sample prepared with a rapid quenching (Insets: the sample look and heating curve).

and flexible (in terms of shape and size) samples [33,34].

Figure 5(a) depicts the influence of various concentration of Ag NPs in the density and molar volume of the synthesized first series of samples. The reduced density suggested the increment of the non-bridging oxygen (NBO) in the network structure. Conversely, the enhanced molar volume could be ascribed to elongation of the bonds within the network. Figure 5(b) represents the variation in the density and molar volume versus Ag NPs content of the second series of samples. The enhanced density and the reduced molar volume were ascribed to the increment of the bridging oxygen (BO) [35] and the shrinkage of the bonds length, respectively. This explained why the structure of the synthesized samples (Series 2) became more compact and rigid.

Figure 6(a) and (b) illustrate the variation in the average molecular weight and the inter-atomic distance with Ag NPs concentration for the first and second series, respectively. The network described to be very tightly packed when the inter-atomic distance reduced with the enhancement of the average molecular weight. The observed increased values in r_i (Ho^{3+} - Ho^{3+} distance) and M_{av} (for the first series) and the reduced values in r_i and M_{av} (for the second series) were ascribed to the structural modification around Ho^{3+} due to the replacement of phosphorous having molecular weight of 141.94 g/mol by AgCl (143.32 g/mol) and pure Ag (107.87 g/mol), respectively.

Figure 7(a) and (b) shows the influence of the varying Ag NPs content on the polaron radius and Ho^{3+} field strength of all prepared samples. The field strength and polaron radius revealed an opposite trend with the

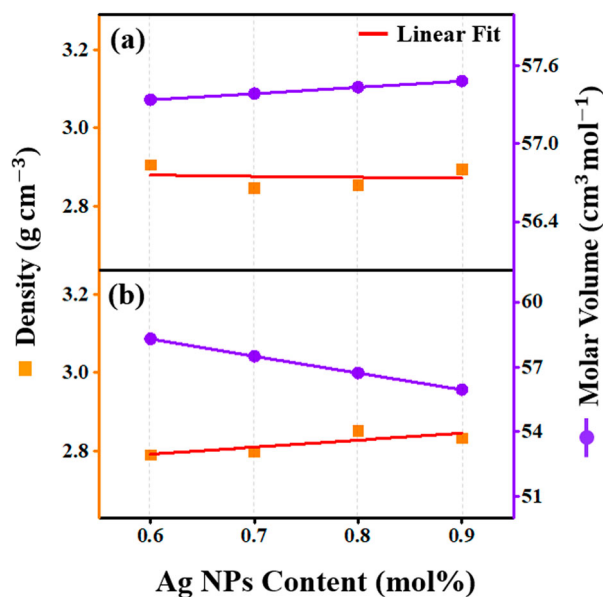


Figure 5. The Ag NPs contents dependent variation of the density and molar volume of the proposed glass-ceramics (a) Series I and (b) Series II.

increase in Ag NPs content. This observation described the network alteration surrounding Ho^{3+} where the polaron (movement of electron with a matrix deformation due to the interaction of the electron with the polar phonons cloud) associates with the matrix covalency and electrovalency (recognized from the field strength). In the first case (Figure 7-a), the reduced trend of the Ho^{3+} field strength indicating the matrix electrovalency nature which assisted the formation and growth of polaron. Conversely, in the second case (Figure 7-b), the couplings of electrons with matrix polar phonons cloud

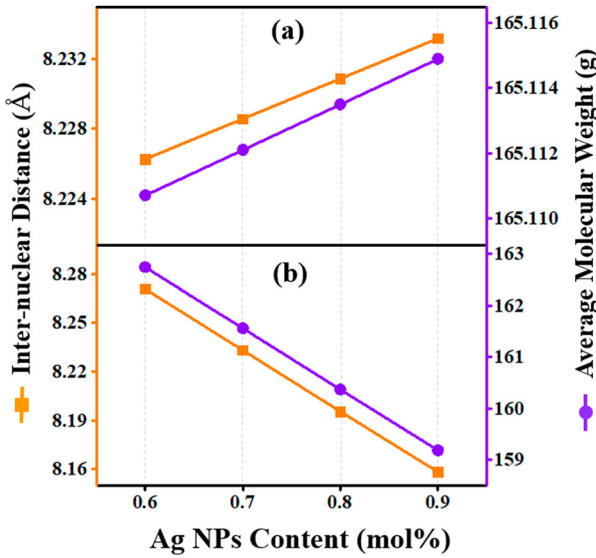


Figure 6. The Ag NPs contents dependent variation of the inter-nuclear distance and average molecular weight of the proposed glass-ceramics (a) Series I and (b) Series II.

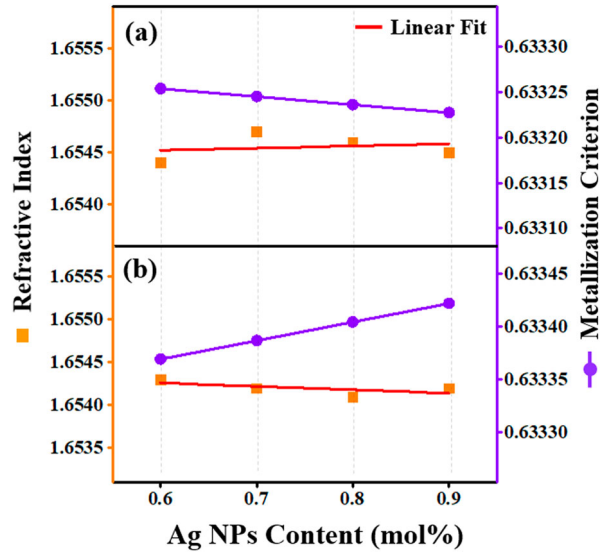


Figure 8. The Ag NPs contents dependent variation of the refractive index and metallization criterion of the proposed glass-ceramics (a) Series I and (b) Series II.

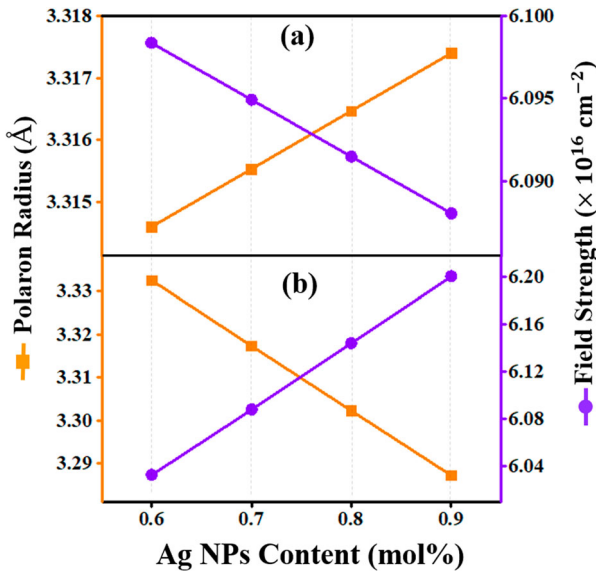


Figure 7. The Ag NPs contents dependent variation of the polaron radius and field strength of the proposed glass-ceramics (a) Series I and (b) Series II.

(polaron) was weak due to the covalent type of network (known from the field strength) resulting in the observed decreased in the polaron radius and increased in the field strength. Moreover, the increased trend of polaron radius (first series) suggested the enhancement of the conduction mechanism of these glass-ceramics by the polaron hopping [31,36].

Figure 8 displays the increasing trend (layer a) and decreasing trend (layer b) of the refractive index with the rise of Ag NPs content for the cited series 1 and 2, respectively. The variation of the refractive index was correlated with the molar volume results for the proposed two series of samples wherein the smaller the molar volume the smaller the electron cloud which

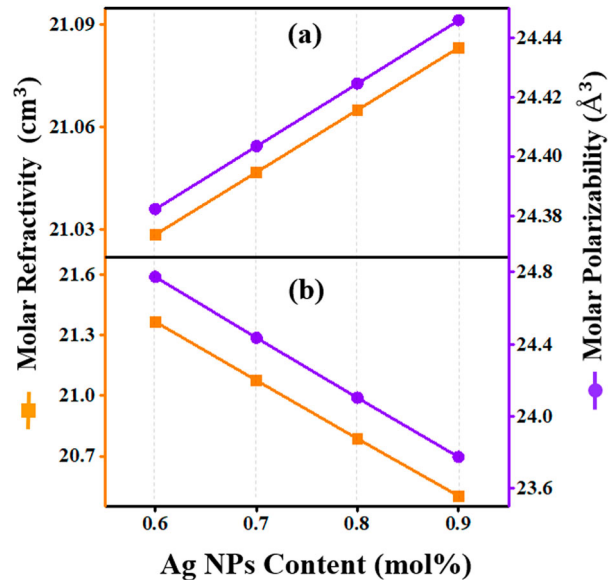


Figure 9. The Ag NPs contents dependent variation of the molar refractivity and polarizability of the proposed glass-ceramics (a) Series I and (b) Series II.

cannot be easily distorted (compared with big electron cloud) lead to reduced polarizability in the system. This distortion was responsible for the dispersion forces (hence lower dispersion). The lower the dispersion, the lesser is the bending or refraction of the light in the material (hence reduced refractive index). Therefore, a structural-optical correlation was established in the systems under study.

Figure 8(a) and (b) also demonstrate the variation in the metallization criterion with the Ag NPs content for the first and second series, respectively. According to the Herzfeld theory of metallization [37], materials with a metallization criterion close to 1 are typical insulators

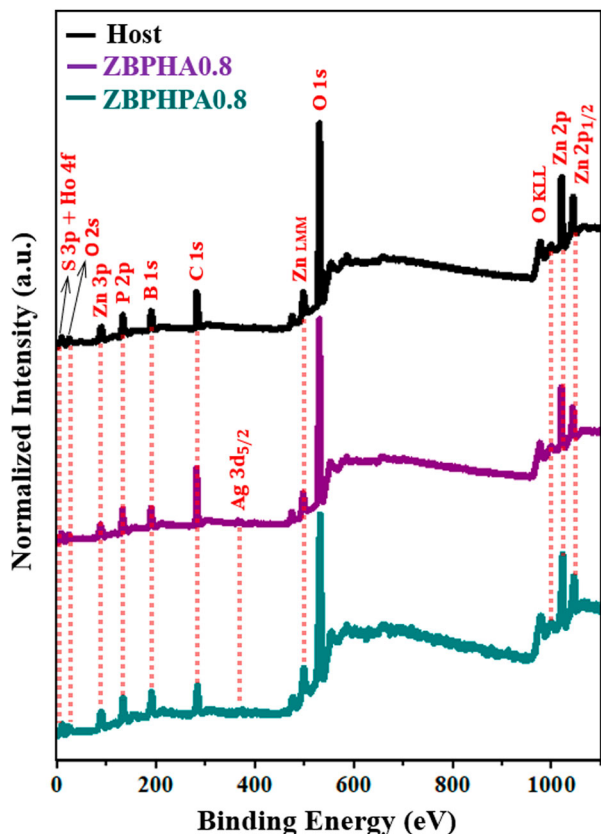


Figure 10. The XPS spectra of the ZBPFA0.8, ZBPHPA0.8 and host ($39.5\text{P}_2\text{O}_5 - 30\text{B}_2\text{O}_3 - 30\text{ZnSO}_4 - 0.5\text{Ho}_2\text{O}_3$) samples.

while materials with smaller value of metallization criterion close to zero reveals metallic features. In this work, the reduction (a) and enhancement (b) in metallization criterion were in well agreement with the earlier finding of polaron hopping contribution in the conduction mechanism.

Figure 9 represents the Ag NPs content dependent molar refractivity and molar polarizability for all synthesized series (a) and (b). The molar refraction determined by the Lorentz-Lorenz equation (Table 2) using the values of refractive index and molar volume measured the total polarizability of a mole of the material. The obtained increasing (a) and decreasing (b) trends of molar refractivity and polarizability were consistent with the density, molar volume, polaron radius, field strength, and refractive index results, reconfirming the revelation of a structural-optical interrelationships in the proposed system.

Figure 10 shows the XPS spectra of the ZBPFA0.8 (Series I), ZBPHPA0.8 (Series II) sample with Ag NPs and the host ($39.5\text{P}_2\text{O}_5 - 30\text{B}_2\text{O}_3 - 30\text{ZnSO}_4 - 0.5\text{Ho}_2\text{O}_3$) glass-ceramic without containing Ag NPs. The observed peaks were indexed using the elemental library in the CasaXPS software which revealed the presence of the elements Ho, S, Zn, P, B, O and Ag (for ZBPFA0.8 and ZBPHPA0.8) in the glass-ceramic network. The observed C1s XPS peak around 285 eV was also reported elsewhere [38,39].

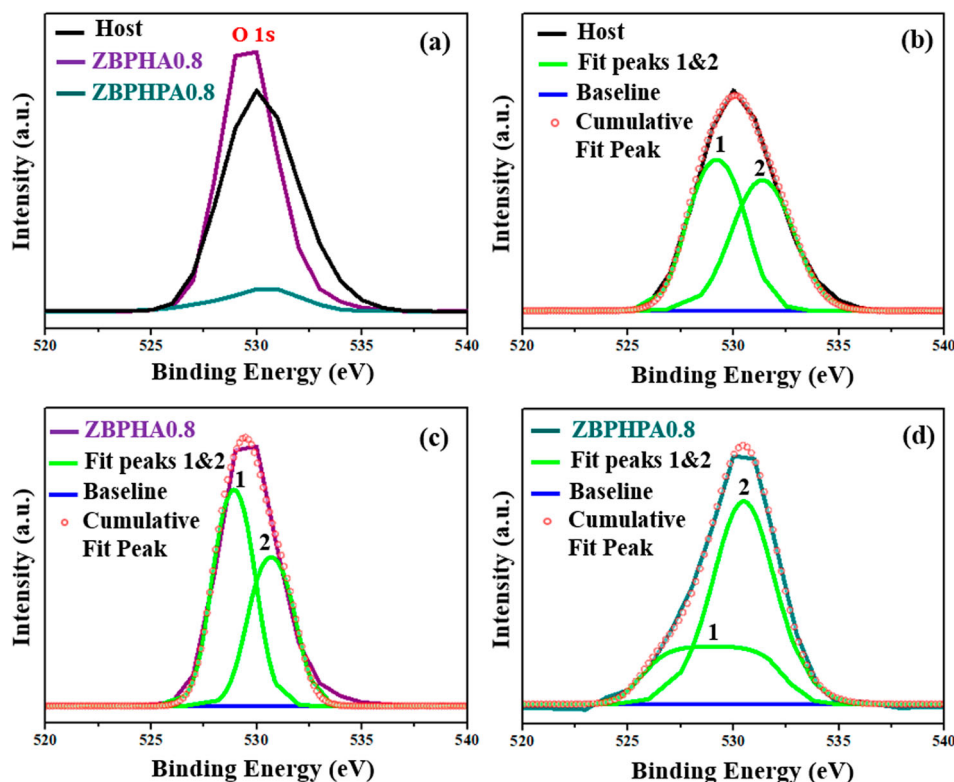


Figure 11. (a) The XPS O1s peak of the ZBPFA0.8 and ZBPHPA0.8 compared to the host sample. (b), (c) and (d) are the Lorentzian-Gaussian fits of the O1s peak for the host, ZBPFA0.8 and ZBPHPA0.8 glass-ceramics, respectively.

Figure 11(a) displays the magnified view of the O1s XPS spectral profile of ZBPHA0.8 (Series I), ZBPHPA0.8 (Series II) and the host glass-ceramics. The XPS intensity of this oxygen peak for ZBPHA0.8 was enhanced and for ZBPHPA0.8 was reduced compared to that of the host. This revelation can be ascribed to the conversion of the NBO to the BO and vice versa, indicating the network structure modifications of the produced glass-ceramics. Additionally, the O1s peak profile was fitted to the double Lorentzian–Gaussian (peaks 1 and 2) as shown in Figure 11(b), (c) and (d). The recorded low value of the binding energy for the peak (1) and high binding energy value for the peak (2) corresponded to the numbers of NBO and BO, respectively [38]. Again, the areas under these two fitted peaks were used to estimate the ratio of the BO to the NBO + BO occurrences [31,38]. The reduction in the BO:NBO + BO value (0.428) for the ZBPHA0.8 (Series I) sample compared to that of the host glass-ceramic (0.487) clearly indicated the significant role of the Ag NPs embedment into the glass-ceramic network, responsible for the generation of more NBO and structural alterations. Conversely, the increase in the BO:NBO + BO value (0.670) for the ZBPHPA0.8 (Series II) sample compared to that of the host glass-ceramic (0.487) showed the considerable opposite effects of the Ag NPs inclusion into the glass-ceramic matrix, accountable for the generation of more BO and associated structural changes. Based on these findings, it can be asserted that by changing the Ag NPs incorporation strategies and contents together with the thermal annealing conditions, the overall properties of the studied glass-ceramics can totally be tailored with different order of magnitudes, implying their viability for various applications. In short, the obtained consistent correlation in the analysed physical parameters and XPS spectra of the proposed glass-ceramic clearly clarified the considerable role of Ag NPs embedment with opposing effects (in order of magnitudes for the Series I and II) in terms of the local structure modifications.

4. Conclusions

For the first time we compared various physical properties of Ho³⁺ activated zinc-sulfo-boro-phosphate glass-ceramics containing different amounts of Ag NPs nucleated via two different strategies. The local network features around the Ho³⁺ was found to be sensitive to customization approach. Interestingly, the incorporation of Ag NPs through pure Ag nanopowder was different from redox assisted nucleation from AgCl. On top, the heat treatment history so called the thermal annealing was shown to play a paramount role on the overall properties modification of the prepared glass-ceramics. Thus, a strong relationship among the quenching procedure, NPs nucleation strategy, physical and structural characteristics can be defined. The measured density and refractive index were used to

determine some significant physical parameters such as molar volume, ionic concentration, inter ionic distance, polaron radius, field strength, molar refractivity, molar polarizability and metallization criterion. The O1s XPS peak was analyzed to evaluate the ratio of bridging to the non-bridging oxygen present in the host matrix. The present findings may promote further studies on the sensitization and optimization of diverse oxide based glass and glass-ceramics included with different LIs and metal nanostructures beneficial for device applications.

Acknowledgements

The authors appreciate the technical and financial support from UTM, Taibah University, and the Ministry of Higher Education Malaysia through the research grant KPT/FRGS Vot. 5F050 and UTMFR 20H65.

Disclosure statement

No potential conflict of interest was reported by the author(s).

Funding

The authors appreciate the technical and financial support from UTM, Taibah University, and the Ministry of Higher Education Malaysia through the research [grant numbers KPT/FRGS Vot. 5F050 and UTMFR 20H65].

ORCID

Areej S. Alqarni  <http://orcid.org/0000-0003-0096-8153>
S. K. Ghoshal  <http://orcid.org/0000-0002-3180-6790>

References

- [1] Li B, Liang J, Sun L, et al. Cyan-emitting Ba₃Y₂B₆O₁₅:Ce³⁺, Tb³⁺ phosphor: a potential color converter for near-UV-excited white LEDs. *J. Lumin.* 2019;211:388–393. doi:10.1016/j.jlumin.2019.04.001.
- [2] Chen R, Tian Y, Li B, et al. Efficient 2 μm emission in Nd³⁺/Ho³⁺ co-doped silicate-germanate glass pumped by common 808 nm LD. *Opt. Laser Technol.* 2017;89:108–113. doi:10.1016/j.optlastec.2016.09.036.
- [3] Xia J, Tian Y, Li B, et al. Enhanced 2.0 μm emission in Ho³⁺/Yb³⁺ co-doped silica-germanate glass. *Infrared Phys. Technol.* 2017;81:17–20. doi:10.1016/j.infrared.2016.10.013.
- [4] Kumar BV, Sankarappa T, Kumar MP, et al. Electronic transport properties of mixed transition metal ions doped borophosphate glasses. *J. Non. Cryst. Solids.* 2009;355:229–234. doi:10.1016/j.jnoncrysol.2008.11.018.
- [5] Pang XG, Eeu TY, Leong PM, et al. Structural and luminescence study of rare earth and transition metal ions doped lead zinc borophosphate glasses. *Adv. Mater. Res.* 2014;895:280–283. doi:10.4028/www.scientific.net/AMR.895.280.
- [6] Elbatal FH, Ibrahim S, Abdelghany AM. Optical and FTIR spectra of NdF₃-doped borophosphate glasses and effect of gamma irradiation. *J. Mol. Struct.* 2012;1030:107–112. doi:10.1016/j.molstruc.2012.02.049.

- [7] Linganna K, Narro-García R, Desirena H, et al. Effect of P2O5 addition on structural and luminescence properties of Nd³⁺-doped tellurite glasses. *J. Alloys Compd.* **2016**;684:322–327. doi:10.1016/j.jallcom.2016.05.082.
- [8] Swapna K, Mahamuda S, Rao AS, et al. Visible luminescence characteristics of Sm³⁺ doped zinc alumino bismuth borate glasses visible luminescence characteristics of Sm³⁺ doped zinc alumino. *J. Lumin.* **2015**;146:288–294. doi:10.1016/j.jlumin.2013.09.035.
- [9] Jupri SA, Ghoshal SK, Omar MF, et al. Spectroscopic traits of holmium in magnesium zinc sulfophosphate glass host: Judd – Ofelt evaluation. *J. Alloys Compd.* **2018**;753:446–456. doi:10.1016/j.jallcom.2018.04.218.
- [10] Zhou M, Zhou Y, Su X, et al. Around 2 μm fluorescence and energy transfer in Tm³⁺/Ho³⁺ co-doped tellurite glass. *J. Non. Cryst. Solids.* **2018**;481:344–351. doi:10.1016/j.jnoncrysol.2017.11.015.
- [11] Kochanowicz M, Žmojda J, Miluski P, et al. Structural and luminescent properties of germanate glasses and double-clad optical fiber co-doped with Yb³⁺/Ho³⁺. *J. Alloys Compd.* **2017**;727:1221–1226. doi:10.1016/j.jallcom.2017.08.243.
- [12] Suresh B, Zhydachevskii Y, Brik MG, et al. Amplification of green emission of Ho³⁺ ions in lead silicate glasses by sensitizing with Bi³⁺ ions. *J. Alloys Compd.* **2016**;683:114–122. doi:10.1016/j.jallcom.2016.05.056.
- [13] Henderson B, Imbusch GF. *Optical spectroscopy of inorganic solids.* Oxford: Clarendon Press; **1989**.
- [14] Walsh BM. Judd-Ofelt theory: principles and practices, in: *Judd-Ofelt Theory Princ. Pract.*, NASA langley research center, Hampton, USA, 2006. doi:10.1007/1-4020-4789-4.
- [15] Pascuta P, Pop L, Stefan R, et al. The impact of Ag and Cu nanoparticles on optical and magnetic properties of new Tb₂O₃-PbO-TeO₂ glass ceramic system. *J. Alloys Compd.* **2019**;799:442–449. doi:10.1016/j.jallcom.2019.05.316.
- [16] Fang Y, Meng S, Hou J, et al. Experimental study of growth of silver nanoparticles embedded in Bi₂O₃-SiO₂-B₂O₃ glass. *J. Alloys Compd.* **2019**;809:151725. doi:10.1016/j.jallcom.2019.151725.
- [17] Kindrat II, Padlyak BV, Kukliński B, et al. Effect of silver co-doping on enhancement of the Sm³⁺ luminescence in lithium tetraborate glass. *J. Lumin.* **2019**;213:290–296. doi:10.1016/j.jlumin.2019.05.045.
- [18] Moustafa SY, Sahar MR, Ghoshal SK. Spectroscopic attributes of Er³⁺ ions in antimony phosphate glass incorporated with Ag nanoparticles: Judd-Ofelt analysis. *J. Alloys Compd.* **2017**;712:781–794. doi:10.1016/j.jallcom.2017.04.106.
- [19] Barnes WL, Dereux A, Ebbesen TW. Surface plasmon sub-wavelength optics. *Nature.* **2003**;424:824–830. doi:10.1038/nature01937.
- [20] Zhang Z, Wang Z, He S, et al. Redox reaction induced Ostwald ripening for size- and shape-focusing of palladium nanocrystals. *Chem. Sci.* **2015**;6:5197–5203. doi:10.1039/c5sc01787d.
- [21] Danmallam IM, Ghoshal SK, Ariffin R, et al. Europium ions and silver nanoparticles co-doped magnesium-zinc-sulfophosphate glasses: Evaluation of ligand field and Judd-Ofelt parameters. *J. Lumin.* **2019**;216:116713. doi:10.1016/j.jlumin.2019.116713.
- [22] Ahmadi F, Hussin R, Ghoshal SK. Spectroscopic attributes of Sm³⁺ doped magnesium zinc sulfophosphate glass: effects of silver nanoparticles inclusion. *Opt. Mater. (Amst).* **2017**;73:268–276. doi:10.1016/j.optmat.2017.08.021.
- [23] Soltani I, Hraiech S, Horchani-Naifer K, et al. Effect of silver nanoparticles on spectroscopic properties of Er³⁺ doped phosphate glass. *Opt. Mater. (Amst).* **2015**;46:454–460. doi:10.1016/j.optmat.2015.05.003.
- [24] Vijayakumar R, Marimuthu K. Luminescence studies on Ag nanoparticles embedded Eu³⁺ doped boro-phosphate glasses. *J. Alloys Compd.* **2016**;665:294–303. doi:10.1016/j.jallcom.2016.01.049.
- [25] Soltani I, Hraiech S, Elhouichet H, et al. Growth of silver nanoparticles stimulate spectroscopic properties of Er³⁺ doped phosphate glasses: heat treatment effect. *J. Alloys Compd.* **2016**. doi:10.1016/j.jallcom.2016.06.027.
- [26] Yamusa YA, Hussin R, Shamsuri WNW. Physical, optical and radiative properties of CaSO₄ – B₂O₃ – P₂O₅ glasses doped with Sm³⁺ ions. *Chinese J. Phys.* **2018**;56:932–943. doi:10.1016/j.cjph.2018.03.025.
- [27] Kesavulu CR, Kim HJ, Lee SW, et al. Optical spectroscopy and emission properties of Ho³⁺-doped gadolinium calcium silicoborate glasses for visible luminescent device applications. *J. Non. Cryst. Solids.* **2017**;474:50–57. doi:10.1016/j.jnoncrysol.2017.08.018.
- [28] Yamusa YA, Hussin R, Shamsuri WNW, et al. Impact of Eu³⁺ on the luminescent, physical and optical properties of BaSO₄-B₂O₃- P₂O₅ glasses. *Optik (Stuttg).* **2018**;164:324–334. doi:10.1016/j.ijleo.2018.03.019.
- [29] Said Mahraz ZA, Sahar MR, Ghoshal SK. Band gap and polarizability of boro-tellurite glass: influence of erbium ions. *J. Mol. Struct.* **2014**;1072:238–241. doi:10.1016/j.molstruc.2014.05.017.
- [30] Usman A, Halimah MK, Latif AA, et al. Influence of Ho³⁺ ions on structural and optical properties of zinc borotellurite glass system. *J. Non. Cryst. Solids.* **2018**;483:18–25. doi:10.1016/j.jnoncrysol.2017.12.040.
- [31] Alqarni AS, Hussin R, Alamri SN, et al. Tailored structures and dielectric traits of holmium ion-doped zinc-sulpho-boro-phosphate glass ceramics. *Ceram. Int.* **2020**;46:3282–3291. doi:10.1016/j.ceramint.2019.10.034.
- [32] Martynov KV, Zakharova EV, Stefanovsky SV, et al. The effect of phosphate melt cooling rate on phase composition and leach resistance of final waste form. *MRS Adv.* **2018**;3:1085–1091. doi:10.1557/adv.2017.616.
- [33] Deopa N, Rao AS, Gupta M, et al. Spectroscopic investigations of Nd³⁺ doped Lithium lead alumino borate glasses for 1.06 μm laser applications. *Opt. Mater. (Amst).* **2018**;75:127–134. doi:10.1016/j.optmat.2017.09.047.
- [34] Reza Dousti M, Amjad RJ, Hosseinian S R, et al. Photoluminescence study of Sm³⁺-Yb³⁺ co-doped tellurite glass embedding silver nanoparticles. *J. Lumin.* **2015**;159:100–104. doi:10.1016/j.jlumin.2014.10.060.
- [35] Venkateswarlu M, Mahamuda S, Swapna K, et al. Holmium doped lead tungsten tellurite glasses for green luminescent applications. *J. Lumin.* **2015**;163:64–71. doi:10.1016/j.jlumin.2015.02.052.
- [36] Alqarni AS, Hussin R, Ghoshal SK, et al. Intense red and green luminescence from holmium activated zinc-sulpho-boro-phosphate glass: Judd-Ofelt evaluation. *J. Alloys Compd.* **2019**;808:151706. doi:10.1016/j.jallcom.2019.151706.
- [37] Herzfeld KF. On atomic properties which make an element a metal. *Phys. Rev.* **1927**;29:701. doi:10.1103/physrev.29.701.
- [38] Das S, Ghosh A. Structure and electrical properties of vanadium boro-phosphate glasses. *J. Non. Cryst. Solids.* **2017**;458:28–33. doi:10.1016/j.jnoncrysol.2016.12.012.
- [39] Wang Y, Yu Y, Zou Y, et al. Broadband visible luminescence in tin fluorophosphate glasses with ultra-low glass transition temperature. *RSC Adv.* **2018**;8:4921–4927. doi:10.1039/c7ra13366a.